Numerical investigation of lobopodia-based 3D cell migration

Francisco Serrano-Alcalde[a], José Manuel García-Aznar[a] and María José Gómez-Benito[a,*]

[a]Multiscale in Mechanical and Biological Engineering (M2BE), Aragón Institute of Engineering Research (I3A), University of Zaragoza, Zaragoza, Spain

Corresponding author

Gómez-Benito, María José

Aragón Institute of Engineering Research (I3A), University of Zaragoza

Poeta Mariano Esquillor, s/n street

50018 Zaragoza (Spain)

Tel.: +34 876 555 237

Email: gomezmj@unizar.es

Abstract

Different cell migration modes have been identified in 3D environments, e.g., modes incorporating lamellopodia or blebs. Recently, a new type of cellular migration has been investigated: lobopodia-based migration, which appears only in three-dimensional matrices under certain conditions. The cell creates a protrusion through which the nucleus slips, dividing the cell into two parts (front and rear) with different hydrostatic pressures. In this work, we elucidate the mechanical conditions that favour this type of migration.

One of the hypotheses about this type of migration is that it depends on the mechanical properties of the extracellular matrix. That is, lobopodia-based migration is dependent on whether the extracellular matrix is linearly elastic or non-linearly elastic.

To determine whether the mechanical properties of the extracellular matrix are crucial in the choice of cell migration mode and which mechanotransduction mechanism the cell might use, we develop a finite element model. From our simulations, we identify two different possible mechanotransduction mechanisms that could regulate the cell to switch from a lobopodial to a lamellipodial migration mode. The first relies on a differential pressure increase inside the cytoplasm while the cell contracts, and the second relies on a change in the fluid flow direction in non-linearly elastic extracellular matrices but not in linearly elastic matrices. The biphasic nature of the cell has been determined to mediate this mechanism and the different behaviours of cells in linearly elastic and non-linearly elastic matrices.

keywords

lobopodia, mechanotransduction, cell migration, poroelasticity, ECM mechanical properties

1. Introduction

Cell migration is essential for many processes, such as embryogenesis, morphogenesis, to maintain tissue regeneration and cancer cell progression. In recent years, several studies have investigated the relationship between the mechanical properties of the extracellular matrix (ECM) and the mechanisms of cellular migration [1, 2, 3]. Understanding how and why cells are able to sense the ECM stiffness and select the best migration strategy have become crucial for progress in these areas of research.

Cell migration in two dimensions (2D) has been extensively described in previous experimental works [4]. These studies have revealed some basic migration mechanisms, such as lamellipodia protrusion, adhesion-mediated traction [5] and actomyosin contractility [6, 7]. In addition, there are different studies in 2D and in three dimensions (3D) relating the mode of cell migration with the mechanical properties of the ECM [2, 8, 9, 10, 11]. These mechanisms depend on the cell type and their physical environments. To better understand the cellular behaviour, several authors studied the influence of the ECM molecular composition [12], the density and orientation of fibres, the fibre-cell interaction [13, 14, 15], the bulk and local stiffness of the ECM [16], the dynamic of actin filaments [17, 18] and the mechanical response of the ECM [8].

However, cell movement mainly occurs in 3D, where cells normally adopt two modes of migration, based on lamellipodia or blebs, depending on the degree of adhesion [19]. Recently, Petrie et al. [8] proposed a new mode of single cell migration, lobopodia-based migration, which takes place only in 3D matrices. In this migration mode, the nucleus has a relevant role. The effect of the nucleus has been studied in previous works for different situations [20, 21]. In this case, the nucleus acts as a piston dividing the cell into two parts with different pressures. The internal pressure in the leading edge is three times larger in lobopodia-based migration than in lamellipodia-based migration [10]. In lamellipodia-based migration, the cell uses different lamellae to move instead of a single large cylindrical protrusion (lobopodium). The possibility of mea-

suring the internal pressure of cells [22] addresses one of the largest differences found between these two migration modes.

Petrie et al. [8, 10] showed that a single fibroblast may switch from actin-driven lamellipodial protrusion to a nuclear piston lobopodia-driven mode of migration. This migration mode depends on the mechanical properties of the ECM, primarily the deformation of the matrix. In fact, whether the ECM is linearly elastic or non-linearly elastic is an essential factor. To elucidate when and where the cell adopts this lobopodial migration mode, the authors carried out experiments with different ECMs [8]. Fibroblasts were embedded in three linearly elastic and non-linearly elastic matrices with different stiffnesses, ranging from 8 to 647 Pa. The ECM was treated to maintain its architecture and change its stiffness and behaviour from linearly elastic or non-linearly elastic. An additional ECM with a higher elastic modulus was also analysed (10 kPa). The authors found no correlation between the migration mode and stiffness of the ECM. However, they found a strong correlation between the ECM non-linear or linear elasticity and the migration mode. Their main conclusion was that the mechanical properties of the ECM are related to the mode of cell migration. For non-linearly elastic matrices, migration occurs via the lamellipodia; however, for linearly elastic matrices, lobopodia predominate in migration. It is known that RhoA, ROCK and myosin II govern intrinsically large protrusions, but why a combination of these signals does not appear in non-linearly elastic ECMs is still unclear. Furthermore, no correlation between the ECM stiffness and the mode of migration was found [8].

Thus, the aim of this work is to elucidate how the mechanical properties and behaviour of the ECM may influence the cell migration mode and why cells adopt a lamellipodial migration mode in non-linearly elastic matrices and a lobopodial mode in linearly elastic matrices. In fact, we hypothesize about the role of the poroelastic behaviour of the cell as a possible mechanotransduction mechanism that could distinguish the impact of different regulatory effects of the surrounding matrix.

2. Materials and Methods

We simulate the experiment developed by Petrie et al. [8] in which a single cell is embedded in different ECMs. A sufficiently large ECM is simulated to avoid border effects. The cell is in the centre of the ECM, and its geometry is a simplified lobopodial geometry (Figure 1). This geometry is approximated from typical lobopodia-based migration behaviour, as shown by Petrie et al. [10]. The model is implemented in commercial finite element (FE) software (ABAQUS).

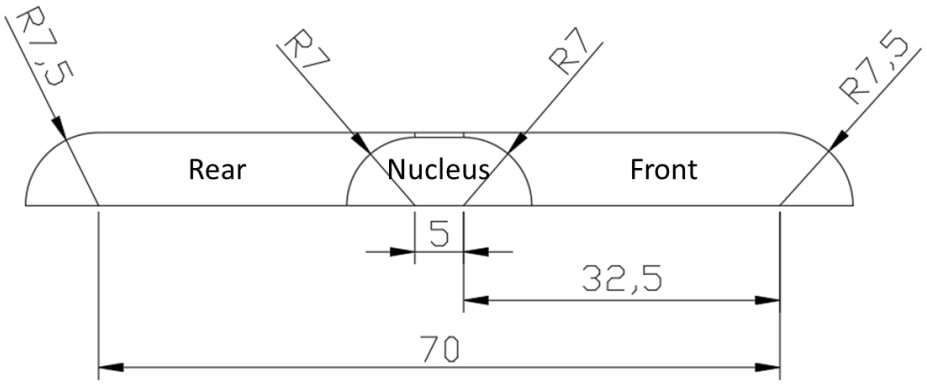

Figure 1: Axisymmetric cell section with a simplified lobopodial geometry (units: μm).

We simulate four different extracellular matrices (Table 1). Two of them have a constant Young's modulus: a cell-derived matrix (CDM) [8] and a trypsinized CDM, both without strain-dependent behaviour and with an elastic modulus of 627 and 8 Pa, respectively. The other two ECMs initially have the same mechanical properties but with a strain-dependent behaviour when the cell starts to deform. Herein, the non-trypsinized CDM matrix is considered the high-stiffness linearly elastic matrix, and the non-trypsinized matrix with strain-dependent behaviour is considered the high-stiffness non-linearly elastic matrix. The trypsinized CDM matrices with an elastic modulus of 8 Pa are considered the low-stiffness linearly and non-linearly elastic matrices.

Matrix	Initial Young's modulus (Pa)	Strain-dependent?
Low stiffness, linearly elastic	8	No
Low stiffness, non-linearly elastic	8	Yes
High stiffness, linearly elastic	627	No
High stiffness, non-linearly elastic	627	Yes

Table 1: Summary of the simulated ECM properties [8].

We fix the Poisson's ratio of the ECM as 0.48 following Petrie et al. [8]. As a first approach, we assume finite strains in all simulations. All linearly elastic matrices are modelled as an elastic material defined by a Young's modulus and Poisson's ratio. We assume a fibrous hyperelastic material in the non-linearly elastic ECMs [23, 24]. The fibres are assumed to be randomly distributed in the ECM, thus an isotropic behaviour can be considered [25]. This model captures the major features of the material properties of collagen gels, including non-linear elasticity.

For collagen hydrogels, we use the strain energy function for fibrous hyperelastic materials from Holzapfel-Gasser-Ogden [26]:

$$U = C\left(\hat{I}_1 - 3\right) + \frac{1}{D}\left(\frac{\left(J^{el}\right)^2 - 1}{2} - \ln J^{el}\right) + \frac{k_1}{2k_2}\sum_{\alpha=1}^{N}\left\{\exp\left[k_2\left\langle \bar{E_\alpha}\right\rangle^2\right] - 1\right\} \tag{1}$$

with

$$\bar{E_\alpha} = \kappa\left(\hat{I}_1 - 1\right) + (1 - 3\kappa)\left(\hat{I}_{4(\alpha\alpha)} - 1\right) \tag{2}$$

where C, D, k_1, k_2 and κ are material parameters, N is the number of families of fibres ($N \leq 3$), $\hat{I}_1$ is the first invariant of the right Cauchy-Green deformation tensor, J^{el} is the elastic volume ratio and $\hat{I}_{4(\alpha\alpha)}$ are pseudo-invariants of the right Cauchy-Green deformation tensor. In our simulations, the parameter κ is fixed to 0.33 assuming a random distribution of fibres, thus resulting in an isotropic material. The values of k_1 and k_2 are $40,000\ Pa$ and 85, respectively,

for the stiff matrix and $1,000\ Pa$ and 20 for the compliant matrix.

To simplify the cell complexity, we simulate only the cytoplasm and the nucleus. The cell nucleus is considered a neo-Hookean hyperelastic material with an initial Young's modulus ten times larger than the stiffness of the cytoplasm following Friedl et al. [27] and Dahl et al. [28] (Table 2) and a Poisson's ratio of 0.49, in accordance with the work of Vaziri et al. [29]. The strain energy function presents the following form:

$$U = C\left(\hat{I}_1 - 3\right) + \frac{1}{D}\left(J^{el} - 1\right)^2 \tag{3}$$

According to the work of Moeendarbary et al. [30], the cytoplasm is simulated as a poroelastic material. Thus, it is composed of two distinct phases, the solid matrix (which is modelled as a linearly elastic material) and the fluid flowing through the solid matrix pores. We consider poroelasticity following the constitutive equation introduced by Biot [31]. This equation relates the total stress tensor $\boldsymbol{\sigma}$ to the strain energy density (a function of the shear G_s and Poisson's ratio ν_s of the drained network) W_s of the solid phase and the pore fluid pressure p following Malandrino and Moeendarbary [32]:

$$\boldsymbol{\sigma} = \frac{2}{J}\frac{\partial W_s}{\partial \mathbf{b}}\mathbf{b} - p\mathbf{I} \tag{4}$$

where J and $\mathbf{b}$ are the determinant and the Left Cauchy-Green tensor both derived from the deformation gradient in the large strain theory. In the solid phase, we assume different Young's moduli depending on the initial stiffness of the ECM following Solon et al. [33]. Cells are able to adjust their internal stiffness to the stiffness of the ECM, clearly indicating mechanical feedback between the cell and its environment. To define the fluid phase, we use the permeability of the solid phase (wherein is implicit the viscosity of the fluid [30]), the volume fraction of the fluid and the specific weight of water. The permeability value is taken from Moeendarbary et al. [30]; however, the volume fraction is chosen as an intermediate value between the previous works of Taber et al. [34], in which the volume fraction was fixed at 0.5, and Moeendarbary

et al. [30], in which the volume fraction was fixed at 0.75 of the fluid. All cytoplasmic properties are shown in Table 2.

	Cell in a compliant ECM	Cell in a stiff ECM
Young's modulus of the cytoplasmic solid phase [35]	100 Pa	2500 Pa
Poisson's ratio of the cytoplasmic solid phase	0.4	0.4
Permeability of the cytoplasmic solid phase [30]	$4 \cdot 10^{-15} \ \frac{m^4}{N \cdot s}$	$4 \cdot 10^{-15} \ \frac{m^4}{N \cdot s}$
Volume fraction of fluid in the cytoplasm [34, 30]	0.6	0.6
Young's modulus of the cell nucleus [27, 28]	1 kPa	10 kPa
Poisson's ratio of the cell nucleus [29]	0.49	0.49

Table 2: Mechanical properties of the cytoplasm and nucleus.

Finally, following other previous work [10], we assume that all the organelles of the cell (Golgi apparatus, endoplasmic reticulum, and so on) are compacted and do not allow fluid flow between the front and the rear part of the cell. Thus, an elastic cytoplasm is simulated surrounding the nucleus and separating the front part of the cytoplasm from the rear part. We assume a linearly elastic material model in this volume, with material properties equal to those of the solid phase of the cytoplasm.

Regarding the FE discretization, the model is simulated using coincident node conditions in the cell and ECM, thus assuming full adhesion between the cell and ECM. We discretize the nucleus, the elastic cytoplasm, the poroelastic cytoplasm and the extracellular matrix with tetrahedral elements (C3D4) (Table 3). The total number of nodes in the final model is $36,990$. Furthermore, a

mesh sensitivity analysis is performed by increasing the total number of nodes up to $369,132$, and the results are equivalent except for a significantly increased calculation time.

Part	Number of elements	Element geometry type	Element material type
ECM	164.224	Tetrahedral C3D4	Solid mechanics
Cytoplasm	44.850	Tetrahedral C3D4P	Solid mechanics and pore pressure
Elastic cytoplasm	3.591	Tetrahedral C3D4	Solid mechanics
Nucleus	6.869	Tetrahedral C3D4H	Hybrid elements

Table 3: Number and type of elements used in the model.

As boundary conditions, we fix all normal displacements of the ECM external surface, and we also fix the flow rate through the cell-matrix interface to zero to avoid the loss of fluid in the cytoplasm, simulating the effect of the cell membrane.

In the simulation, we first apply a predefined stress in the cytoplasm assuming an initial pressure inside the cell [10]. Previous works [35] established an initial pre-stress in the cell that is related to the ECM stiffness. Petrie et al. [10] also measured the hydrostatic pressure of a cell with a lamellipodial migration mode. Thus, we use this pressure to calibrate the initial pressure of the cell. In addition, we simulate 3 seconds to make the internal pressure along the cell homogeneous after the initial pre-stress and to establish the initial equilibrium state.

Finally, for lobopodia-based migration, the cell is not polarized in the same way as lamellipodia-based, and the movement depends on the RhoA, ROCK and myosin II contractility [8]. Furthermore, the myosin II distribution inside the cell for lamellipodia-based migration is homogeneous, while for lobopodia-based migration, the distribution is concentrated forward of the nucleus. Thus,

a different polarization is present and is apparently necessary to maintain cell migration. Accordingly, we apply a constant linear contraction for 20 seconds at the front of the cell to simulate the cell contractility. Due to the behavior of the poroelastic material, we are modeling a dense solid network connecting the nucleus with the trailing edge and we apply the contraction on this solid phase of the cytoplasm. Furthermore, we assume anisotropic contraction of the cell and we only allow cell contractility in the longitudinal direction.

3. Results

We focus our analysis on the pressure in the front part of the cell (where contraction occurs), the ECM strains, the stresses on the cell nucleus and the fluid flow inside the cell. All measurements are taken during cell contraction.

First, we analyse the evolution of pressure in the front part of the cytoplasm. Figures 2a and 2b show the evolution of hydrostatic pressure in the front part of the cytoplasm for the stiff and compliant ECMs, respectively, while the cell contracts. Cell contraction provokes the volume variation of the cell in the longitudinal direction. This added to the coupled effect of the solid phase (compressibility) and the cell-matrix adhesion are the main effects causing the pressure variation. The initial pressure of cells in the stiff matrix is higher than that of cells in the compliant matrix since we apply more pre-stress in the stiffer cytoplasm following the work of Discher et al. [35]. Then, the difference between linearly elastic and non-linearly elastic ECMs can be observed. For the high-stiffness linearly elastic matrix, the pressure increases linearly from the initial 600 Pa to 2000 Pa at the end of the contraction. Nevertheless, for the high-stiffness non-linearly elastic matrix, the pressure starts increasing; however, it subsequently reaches saturation at approximately 1500 Pa. The same tendency is found for the cell in the compliant ECM: in the linearly elastic case, the increase in pressure is maintained; however, in the non-linearly elastic case, the pressure first increases and then reaches saturation.

We also carry out a sensitivity study of the cytoplasmic mechanical proper-

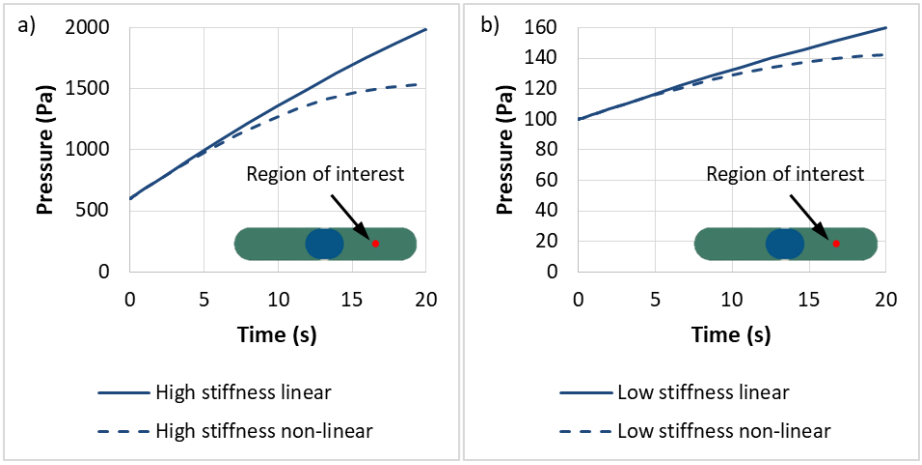

Figure 2: Evolution of the hydrostatic pressure in the front part of the cytoplasm while the cell contracts for high-stiffness (a) and low-stiffness (b) linearly elastic and non-linearly elastic ECMs.

ties. We vary the fluid content, elastic modulus and Poisson's ratio for the cell in the stiffer ECM. We choose a higher and a lower value for each parameter. All the results show the same behaviour of cell pressure, but the values are property dependent. There is a sustained increase in the cytoplasmic pressure when the cell contracts in the linearly elastic ECM and an initial increase and subsequent asymptotic decrease in pressure in the non-linearly elastic ECM (Figure 3). The effects of the elastic modulus and Poisson's ratio of the cytoplasm on the cytoplasmic pressure are higher than those of the fluid volume fraction. Nevertheless, there are slight differences in the pressure for the linearly elastic and non-linearly elastic ECMs.

Second, we analyse the fluid velocity in the cytoplasm during contraction. We find a change in the direction of the fluid flow in the non-linearly elastic case. In the first seconds of contraction, the fluid shifts from the front part to the rear part of the cytoplasm, which undergoes contraction in both the linearly elastic and the non-linearly elastic ECMs. Nevertheless, when the pressure starts to increase in the non-linearly elastic matrices (Figure 2a and 2b), the fluid in the

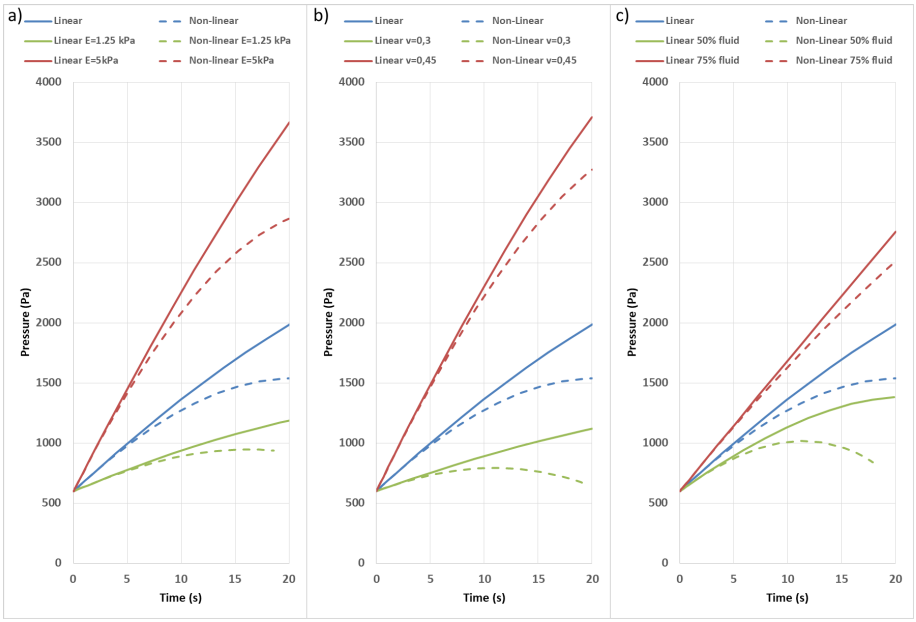

Figure 3: Sensitivity analysis of the cytoplasmic mechanical properties on the cytoplasmic hydrostatic pressure while the cell contracts within high-stiffness linearly elastic and non-linearly elastic ECMs. a) Influence of the elastic modulus of the cytoplasm solid phase; b) influence of Poisson's ratio of the cytoplasm solid phase; c) influence of the fluid volume in the cytoplasm.

cytoplasm changes direction and flows from the nucleus to the front part (Figure 4). This response could activate some mechanotransduction mechanism in the cell to change from a lobopodia-based to a lamellipodia-based migration mode.

We also analyse the role of the mechanical characteristics of the ECM. We focus on the maximum tensile strains (Figure 5) in the ECM for both the linearly elastic and the non-linearly elastic ECMs with high and low elastic moduli. In general, the maximum principal strains are lower in the non-linearly elastic matrices than in the linearly elastic matrices for both high- and low-stiffness matrices. In addition, the strains around the cell are more homogeneously distributed (with values close to 17 %) in the non-linearly elastic ECM. For the linearly elastic ECMs, the distribution is less uniform, and the strain values close

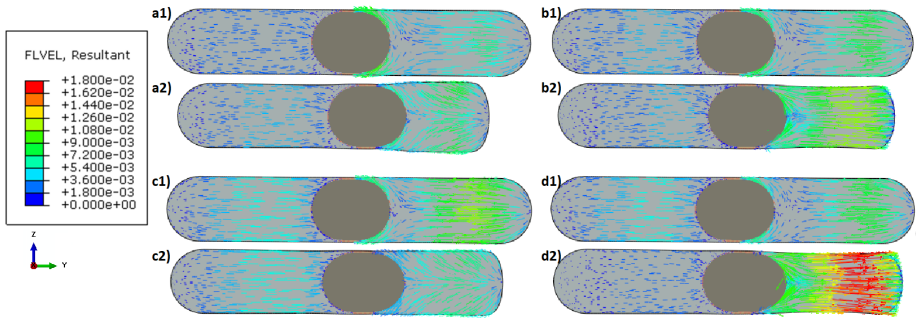

Figure 4: Fluid velocity in the cytoplasm for the a) low-stiffness linearly elastic ECM, b) low-stiffness non-linearly elastic ECM, c) high-stiffness linearly elastic ECM and d) high-stiffness non-linearly elastic ECM at the begining of the contraction (1) and the end of the contraction (2) (units: $\mu m/s$).

to the cell are between 30 and 60 % in the linearly elastic case. The maximum value is at the front of the cell, but the strain distribution away from the cell is very similar for both the linearly elastic and the non-linearly elastic ECMs.

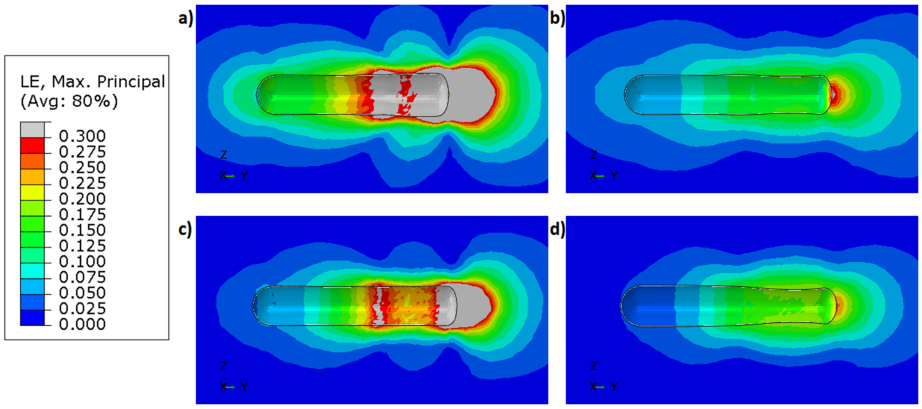

Figure 5: Logarithmic maximum principal strain in the ECM: a) low-stiffness linearly elastic ECM, b) low-stiffness non-linearly elastic ECM, c) high-stiffness linearly elastic ECM and d) high-stiffness non-linearly elastic ECM.

These differences can be attributed to the non-linear or linear elasticity of the ECM. In the case of the linearly elastic matrices, the stiffness remains con-

stant, but for the non-linearly elastic matrices, the elastic modulus of the ECM increases in the zones with high strains, mainly in the front part of the cell (Figure 6).

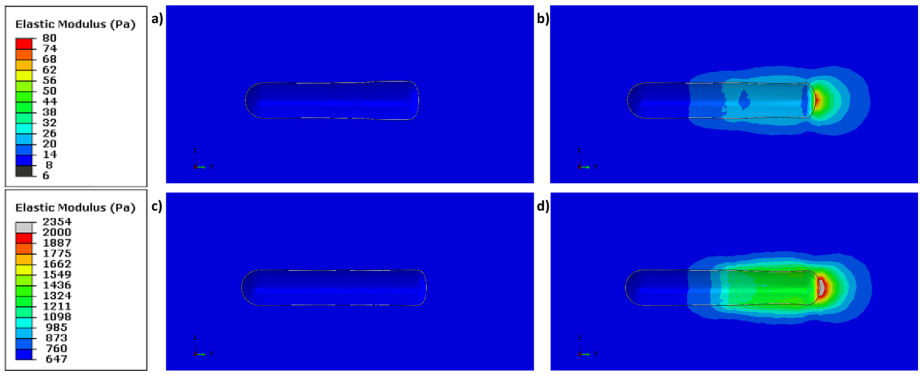

Figure 6: Final equivalent elastic modulus (Pa) of the ECM: a) low-stiffness linearly elastic ECM, b) low-stiffness non-linearly elastic ECM, c) high-stiffness linearly elastic ECM and d) high-stiffness non-linearly elastic ECM.

Finally, we analyse the mechanical state of the cell nucleus related to different cell processes, such as differentiation (Dahl et al. [28]). To study how ECM behaviour could affect the nucleus, if cells migrate in the lobopodia-based mode, we obtain the maximum tensile stress in the cell nucleus (Figure 7). Although the value of the maximum principal stress depends on the ECMs in which cells migrate, we find the same distribution of stresses depending on the mechanical behaviour of the ECM. For the linearly elastic matrices, all the nuclei bear the same tensile stress, while for the non-linearly elastic matrices, the range of values is higher, with a higher tensile stress in the front part of the nucleus and a lower stress in the rear part of the nucleus.

4. Discussion and Conclusions

Different mechanotransduction mechanisms could regulate the cell to change from a lobopodial to a lamellipodial migration mode or vice versa. From our simulation, we hypothesize that the cell capacity to deform the ECM regulates

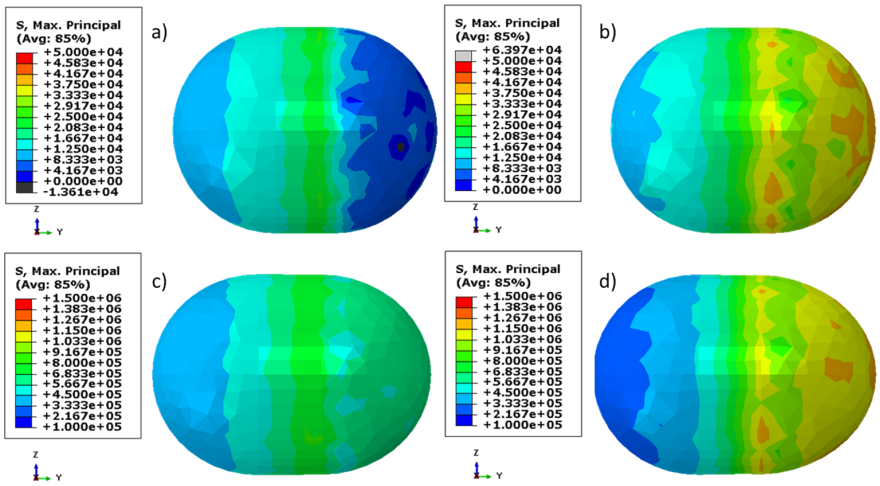

Figure 7: Maximum principal stresses in the nucleus for the a) low-stiffness linearly elastic ECM, b) low-stiffness non-linearly elastic ECM, c) high-stiffness linearly elastic ECM and d) high-stiffness non-linearly elastic ECM (units mPa).

the pressure differences across the cell body. Pressure variation is actively caused by cell contraction, but how easy or not the matrix allows the movement of the cell influences passively the pressure. Somehow, there is a competition between the cell and the extracellular matrix. Therefore, depending on the mechanical response to the cell forces, the pressure differs inside the cell. In fact, these pressure differences could also reorganize the cytoskeleton and consequently define the migratory path [36]. In particular, in our work, we estimate that the first increase in pressure at the beginning of cell contraction and the subsequent decrease could be one factor leading a mechanotransduction mechanism. Additionally, the change in fluid flow inside the cytoplasm when the cell contracts could act as a stimulus that prompts the cell to change to a lamellipodial migration mode. Other authors have hypothesized that cells can select different migration mechanisms depending on the external coefficient of hydraulic resistance associated with the ECM [37]. Under this framework, the mechanism that regulates cell migration is the capacity of the cell to displace the external water in the ECM. Both theories—i.e., that are based on the effect that the

cytoskeleton exerts on the movement of the fluid inside the cell body or that are based on a related effect outside the cell body—can provide new perspectives on how cells regulate their movement.

One of the challenges of computational models of single cells is the mechanical properties of cells and the ECM. It is difficult to obtain an accurate measure of such properties due to the scale and the complexity of testing each single component of the cell separately from the other components. In addition, most works assume different Poisson ratios when measuring the elastic modulus of the cell. For example, Moeendarbary et al. [30], who presented (to our knowledge) the first work in which the cytoplasm is assumed to be a poroelastic material, fixed the Poisson's ratio of the solid phase as 0.3, and Mahaffy et al. [38] studied the effect of different values. This problem is even more important if we are assuming a two-phase material (poroelastic cytoplasm). Thus, in our opinion, it is important to develop and implement computational models because they provide us with information that allows us to qualitatively compare the cell behaviour under different assumptions. In our parametric study, as shown in Figure 3, we can see the different behaviour of the intracellular pressure varying the cytoplasmic properties. For an increasing elastic modulus or Poisson's ratio, the increase in pressure is very similar, but we observe more differences between the linearly elastic and non-linearly elastic ECMs in terms of the increasing elastic modulus of the cytoplasm. In contrast, by decreasing Young's modulus or Poisson's ratio of the cytoplasm, the pressure decreases in both cases, but the differences between the linearly elastic and non-linearly elastic ECMs are higher as Poisson's ratio decreases. Furthermore, the effect of the fluid volume ratio on the cytoplasm is quite similar to that of Poisson's ratio, but the former parameter has a lower impact on the intracellular pressure.

To carry out this work, we make several simplifications in the model due to the absence of available experimental data. First, the role of the membrane is taken into account only to avoid fluid flow between the cell and the ECM; it is not simulated as an active part of the cell. Second, we assume that the cell changes its properties depending on the ECM in which it is embedded. In

fact, Solon et al. [33] demonstrated that the elastic modulus of the cytoplasm changes depending on the substrate properties. However, we decided to simulate these particular ECMs since they are the only ones for which Petrie et al. [10] measured the hydrostatic pressure inside the cell. Finally, the geometry is a simplification of a real cell because of the variability in cell geometry while migrating. This geometry captures the main geometrical features of the cell in its lobopodial migration mode.

In this work, we simulate the experimental work of Petrie et al. [10]. Our aim is to elucidate whether the differences observed in their experiments could be at least partially explained by the water movement through the solid phase of the cytoplasm (featuring a cytoskeleton and macromolecular crowding) [30]. We observe different behaviour in the internal pressure of the cytoplasm, and we also show the effect of the cytoplasmic properties. Another important result is the internal fluid flow of the cell. This flow changes direction depending on the ECM response. The final elastic modulus of the ECM (Figure 6) results in higher stresses in the nucleus for the non-linearly elastic ECM.

Despite all these simplifications, we obtain similar results to those obtained in the experimental work [10]. We use the results of the intracellular pressure in the front part of a lobopodial cell in the CDM matrix (high stiffness, linearly elastic) to validate our results. The experimental value of the pressure is on the order of 2 kPa, which is approximately the value estimated from our numerical predictions in Figure 2. Thus, the model could help to better understand why cells do not use lobopodia-based migration in non-linearly elastic matrices. We identify two possible mechanosensory variables that could regulate the cell changes from the lobopodial to the lamellipodial migration mode, which are the fluid flow and the hydrostatic pressure inside the cytoplasm. Our results show that relevant differences can be found in the fluid flow and the hydrostatic pressure for different behaviours of the extracellular matrix, although we do not analyse how these variables can control cell migration. Certainly, this aspect would require additional study and further simulations.

5. Acknowledgements

This research was supported by the Spanish Ministry of Economy and Competitiveness through project RTI2018-094494-B-C21. This project was partially financed by the European Union (through the European Regional Development Fund).

References

[1] M. H. Zaman, L. M. Trapani, A. L. Sieminski, D. MacKellar, H. Gong, R. D. Kamm, A. Wells, D. A. Lauffenburger, P. Matsudaira, Migration of tumor cells in 3d matrices is governed by matrix stiffness along with cell-matrix adhesion and proteolysis, Proceedings of the National Academy of Sciences 103 (29) (2006) 10889–10894.

[2] P. Friedl, K. Wolf, Plasticity of cell migration: a multiscale tuning model, The Journal of Cell Biology 188 (1) (2010) 11–19.

[3] T. Luque, E. Melo, E. Garreta, J. Cortiella, J. Nichols, R. Farré, D. Navajas, Local micromechanical properties of decellularized lung scaffolds measured with atomic force microscopy, Acta Biomaterialia 9 (6) (2013) 6852 – 6859.

[4] D. A. Lauffenburger, A. F. Horwitz, Cell migration: a physically integrated molecular process, Cell 84 (3) (1996) 359–369.

[5] R. Oria, T. Wiegand, J. Escribano, A. Elosegui-Artola, J. J. Uriarte, C. Moreno-Pulido, I. Platzman, P. Delcanale, L. Albertazzi, D. Navajas, et al., Force loading explains spatial sensing of ligands by cells, Nature 552 (7684) (2017) 219.

[6] A. J. Ridley, M. A. Schwartz, K. Burridge, R. A. Firtel, M. H. Ginsberg, G. Borisy, J. T. Parsons, A. R. Horwitz, Cell migration: integrating signals from front to back, Science 302 (5651) (2003) 1704–1709.

[7] R. Sunyer, V. Conte, J. Escribano, A. Elosegui-Artola, A. Labernadie, L. Valon, D. Navajas, J. M. García-Aznar, J. J. Muñoz, P. Roca-Cusachs, et al., Collective cell durotaxis emerges from long-range intercellular force transmission, Science 353 (6304) (2016) 1157–1161.

[8] R. J. Petrie, N. Gavara, R. S. Chadwick, K. M. Yamada, Nonpolarized signaling reveals two distinct modes of 3d cell migration, The Journal of Cell Biology 197 (3) (2012) 439–455.

[9] D. W. DeSimone, A. R. Horwitz, Many modes of motility, science 345 (6200) (2014) 1002–1003.

[10] R. J. Petrie, H. Koo, K. M. Yamada, Generation of compartmentalized pressure by a nuclear piston governs cell motility in a 3d matrix, Science 345 (6200) (2014) 1062–1065.

[11] R. J. Petrie, K. M. Yamada, Multiple mechanisms of 3d migration: the origins of plasticity, Current Opinion in Cell Biology 42 (2016) 7 – 12, cell dynamics.

[12] O. Moreno-Arotzena, C. Borau, N. Movilla, M. Vicente-Manzanares, J. M. García-Aznar, Fibroblast migration in 3d is controlled by haptotaxis in a non-muscle myosin ii-dependent manner, Annals of Biomedical Engineering 43 (12) (2015) 3025–3039.

[13] R. Sturm, A computer model for the simulation of fiber–cell interaction in the alveolar region of the respiratory tract, Computers in Biology and Medicine 41 (7) (2011) 565–573.

[14] J. Escribano, M. Sánchez, J. García-Aznar, Modeling the formation of cell-matrix adhesions on a single 3d matrix fiber, Journal of theoretical biology 384 (2015) 84–94.

[15] S. I. Fraley, P.-h. Wu, L. He, Y. Feng, R. Krisnamurthy, G. D. Longmore, D. Wirtz, Three-dimensional matrix fiber alignment modulates cell migra-

tion and mt1-mmp utility by spatially and temporally directing protrusions, Scientific reports 5 (2015) 14580.

[16] K. E. Kubow, S. K. Conrad, A. R. Horwitz, Matrix microarchitecture and myosin {II} determine adhesion in 3d matrices, Current Biology 23 (17) (2013) 1607 – 1619.

[17] Y. Inoue, T. Deji, Y. Shimada, M. Hojo, T. Adachi, Simulations of dynamics of actin filaments by remodeling them in shearflows, Computers in Biology and Medicine 40 (11) (2010) 876–882.

[18] S. Hervas-Raluy, J. Garcia-Aznar, M. Gomez-Benito, Modelling actin polymerization: the effect on confined cell migration, Biomechanics and modeling in mechanobiology (2019) 1–11.

[19] V. Te Boekhorst, L. Preziosi, P. Friedl, Plasticity of cell migration in vivo and in silico, Annual review of cell and developmental biology 32 (2016) 491–526.

[20] R. Allena, H. Thiam, M. Piel, D. Aubry, A mechanical model to investigate the role of the nucleus during confined cell migration, Computer methods in biomechanics and biomedical engineering 18 (sup1) (2015) 1868–1869.

[21] F. Serrano-Alcalde, J. M. García-Aznar, M. J. Gómez-Benito, The role of nuclear mechanics in cell deformation under creeping flows, Journal of theoretical biology 432 (2017) 25–32.

[22] R. J. Petrie, H. Koo, Direct measurement of intracellular pressure, Current protocols in cell biology 63 (1) (2014) 12–9.

[23] T. Elsdale, J. Bard, Collagen substrata for studies on cell behavior, The Journal of cell biology 54 (3) (1972) 626–637.

[24] R. Gelman, B. R. Williams, K. Piez, Collagen fibril formation. evidence for a multistep process., Journal of Biological Chemistry 254 (1) (1979) 180–186.

[25] T. C. Gasser, R. W. Ogden, G. A. Holzapfel, Hyperelastic modelling of arterial layers with distributed collagen fibre orientations, Journal of the royal society interface 3 (6) (2006) 15–35.

[26] G. A. Holzapfel, T. C. Gasser, R. W. Ogden, A new constitutive framework for arterial wall mechanics and a comparative study of material models, Journal of elasticity and the physical science of solids 61 (1-3) (2000) 1–48.

[27] P. Friedl, K. Wolf, J. Lammerding, Nuclear mechanics during cell migration, Current Opinion in Cell Biology 23 (1) (2011) 55 – 64, cell structure and dynamics.

[28] K. N. Dahl, A. J. Ribeiro, J. Lammerding, Nuclear shape, mechanics, and mechanotransduction, Circulation Research 102 (11) (2008) 1307–1318.

[29] A. Vaziri, H. Lee, M. K. Mofrad, Deformation of the cell nucleus under indentation: mechanics and mechanisms, Journal of materials research 21 (08) (2006) 2126–2135.

[30] E. Moeendarbary, L. Valon, M. Fritzsche, A. R. Harris, D. A. Moulding, A. J. Thrasher, E. Stride, L. Mahadevan, G. T. Charras, The cytoplasm of living cells behaves as a poroelastic material, Nature materials 12 (3) (2013) 253–261.

[31] M. A. Biot, General theory of three-dimensional consolidation, Journal of Applied Physics 12 (2) (1941) 155–164.

[32] A. Malandrino, E. Moeendarbary, Poroelasticity of living tissues, in: R. Narayan (Ed.), Encyclopedia of Biomedical Engineering, Elsevier, Oxford, 2019, pp. 238 – 245.

[33] J. Solon, I. Levental, K. Sengupta, P. C. Georges, P. A. Janmey, Fibroblast adaptation and stiffness matching to soft elastic substrates, Biophysical Journal 93 (12) (2007) 4453 – 4461.

[34] L. Taber, Y. Shi, L. Yang, P. Bayly, A poroelastic model for cell crawling including mechanical coupling between cytoskeletal contraction and actin polymerization, Journal of mechanics of materials and structures 6 (1) (2011) 569–589.

[35] D. E. Discher, P. Janmey, Y.-l. Wang, Tissue cells feel and respond to the stiffness of their substrate, Science 310 (5751) (2005) 1139–1143.

[36] H. Jiang, S. X. Sun, Cellular pressure and volume regulation and implications for cell mechanics, Biophysical journal 105 (3) (2013) 609–619.

[37] Y. Li, S. X. Sun, Transition from actin-driven to water-driven cell migration depends on external hydraulic resistance, Biophysical Journal 114 (12) (2018) 2965–2973.

[38] R. Mahaffy, S. Park, E. Gerde, J. Käs, C. Shih, Quantitative analysis of the viscoelastic properties of thin regions of fibroblasts using atomic force microscopy, Biophysical Journal 86 (3) (2004) 1777 – 1793.